Hindawi
Advances in High Energy Physics
Volume 2019, Article ID 3902819, 10 pages
https://doi.org/10.1155/2019/3902819

Research Article

Coherent Elastic Neutrino-Nucleus Scattering as a Precision Test for the Standard Model and Beyond: The COHERENT Proposal Case

O. G. Miranda, G. Sanchez Garcia, and O. Sanders

Departamento de Física, Centro de Investigación y de Estudios Avanzados del IPN, Apdo. Postal 14-740, 07000 Ciudad de México, Mexico

Correspondence should be addressed to O. G. Miranda; omr@fis.cinvestav.mx

Received 4 March 2019; Revised 5 July 2019; Accepted 17 July 2019; Published 20 August 2019

Academic Editor: Alessandro Baldini

Several experimental proposals expect to confirm the recent measurement of the coherent elastic neutrino-nucleus scattering (CEvNS). Motivated in particular by the next generation experiments of the COHERENT collaboration, we study their sensitivity to different tests of the Standard Model and beyond. We analyze the resolution that can be achieved by each future proposed detector in the measurement of the weak mixing angle; we also perform a similar analysis in the context of Nonstandard Interaction (NSI) and in the case of oscillations into a sterile neutrino state. We show that future perspectives are interesting for these types of new physics searches.

1. Introduction

Despite the fact that coherent elastic neutrino-nucleus scattering (CEvNS) was proposed more than forty years ago [1], it was only recently that the COHERENT collaboration observed this process for the first time by using a CsI[Na] detector exposed to the neutrino flux generated at the Spallation Neutron Source (SNS) at Oak Ridge National Laboratory [2].

In a CEvNS process, an incident neutrino interacts coherently with the protons and neutrons within the nucleus. As a result, there is an enhancement in the cross-section, which turns out to be quadratic in the number of nucleons. The necessary condition to observe this phenomenon is that the energy of the neutrino must be sufficiently low so that the momentum transfer satisfies $qR << 1$, with R the nuclear radius. Since its first detection, COHERENT data have been studied for different purposes such as measurements of nuclear neutron distributions [3], weak mixing angle [4, 5], neutrino electromagnetic properties [6, 7], and tests of NSI neutrino interactions [6, 8, 9].

In the future, the COHERENT program [10] will include a set of four detectors, each based on different materials and technologies capable of observing low-energy nuclear recoils: the currently used CsI[Na] scintillating crystal, with which CEvNS was detected for the first time, and three future experiments that are still being developed: a set of p-type point-contact Germanium detectors, a single-phase liquid Argon detector, and an array of NaI[Tl] crystals. Each detector has a different threshold, baseline, and mass, all of which are summarized in Table 1. In this work we study the future experimental setups proposed by the COHERENT collaboration in order to test the sensitivity of CEvNS to the weak mixing angle and the search of new physics by two different mechanisms; the first one through the introduction of parameters which describe NSI and the other by introducing the possibility of a specific neutrino flavor to oscillate into a sterile one. The same original experimental proposal [10] introduces a discussion about nonstandard interactions (NSI) as well as implications for dark matter. In this work, for the NSI analysis, we study both nonuniversal and flavor-changing NSI parameters. Different authors have already studied part

Table 1: Current and future experimental setups for the COHERENT collaboration detectors [10].

	T_{thres}	Baseline	Det. Tec.	Fid. Mass
$^{133}Cs^{127}I$	5 keV	19.3 m	Scintillator	14.6 kg
^{72}Ge	5 keV	22 m	HPGe PPC	10 kg
$^{23}Na^{127}I$	13 keV	28 m	Scintillator	2000 kg
^{40}Ar	20 keV	29 m	Liquid scintillator	1000 kg

of the potential of these detectors in a different context [11–16]. Here we focus on the specific configurations reported by the COHERENT collaboration for its future stages [10] to have a complementary forecast that includes cases that have not been covered, such as the future perspectives for the measurement of a weak mixing angle for these detectors.

2. Coherent Elastic Neutrino-Nucleus Scattering

Before discussing the future perspectives for CEvNS in a specific SNS experiment, we present in this section the main characteristics of the neutrino flux, cross-section and form factors involved in the prediction of the number of events measured by a given detector. The neutrino beam used by the COHERENT collaboration consists of ν_e, ν_μ, and $\overline{\nu}_\mu$ fluxes coming from the SNS. These neutrinos are produced by the π^+ decay-at-rest in the form $\pi^+ \longrightarrow \mu^+\nu_\mu$ and thus we have a monoenergetic beam of muon neutrinos, known as "prompt" neutrinos, which can be described by

$$\frac{\mathrm{dN}_{\nu_\mu}}{\mathrm{d}E} = \eta\delta\left(E - \frac{m_\pi^2 - m_\mu^2}{2m_\pi}\right). \tag{1}$$

Eventually, the μ^+'s also decay to produce antimuon neutrinos and electron neutrinos, which together are known as "delayed neutrinos", and which can be modeled, for energies up to 52.8 MeV, as [3]:

$$\frac{\mathrm{dN}_{\overline{\nu}_\mu}}{\mathrm{d}E} = \eta\frac{64E^2}{m_\mu^3}\left(\frac{3}{4} - \frac{E}{m_\mu}\right) \tag{2}$$

$$\frac{\mathrm{dN}_{\nu_e}}{\mathrm{d}E} = \eta\frac{192E^2}{m_\mu^3}\left(\frac{1}{2} - \frac{E}{m_\mu}\right) \tag{3}$$

with $\eta = rN_{POT}/4\pi L^2$ being a normalization factor with $r = 0.08$ the number of neutrinos per flavor, $N_{POT} = 1.76 \times 10^{23}$ the number of protons on target, and L the distance between the source and the detector. The total neutrino flux is considered to be the sum of the three previous contributions. For all our computations we will consider the same total flux, and we set it as equal to that of the first COHERENT measurement [2]; in this way, our comparison of results will be made using the same standard time window.

Regarding the CEvNS cross-section, this has been computed to be [18–21]

$$\left(\frac{d\sigma}{dT}\right)_{\mathrm{SM}}^{\mathrm{coh}} = \frac{G_F^2 M}{\pi}\left[1 - \frac{MT}{2E_\nu^2}\right]\left[Zg_V^p F_Z\left(q^2\right) + Ng_V^n F_N\left(q^2\right)\right]^2. \tag{4}$$

Here, M is the mass of the nucleus, E_ν is the neutrino energy, and T is the nucleus recoil energy; $F_{Z,N}(q^2)$ are the corresponding nuclear form factors, which are especially important at higher momentum transfer, as is the case of neutrinos coming from the SNS. In other cases, as for antineutrinos coming from nuclear reactors, these form factors have a minimal impact due to the low momentum transfer. We have computed our results by using a Helm form factor as well as a symmetrized Fermi one for both protons and neutrons; our results in all cases were the same up to the level of one per thousand, so in what follows, we will consider the Helm form factor for neutrons and the symmetrized Fermi one for protons. The neutral current vector couplings are given by

$$g_V^p = \frac{1}{2} - 2\hat{s}_Z^2$$
$$g_V^n = -\frac{1}{2} \tag{5}$$

where $\hat{s}_Z^2 = \sin^2\theta_W = 0.23865$, which corresponds to the low-energy limit as well. [22].

Recently, a new computation that studies in more detail the cross-section for the case of a nonzero spin nucleus (taking into account the kinematics for relatively high momentum transfer) has been reported [17]. It has been stated that kinematic corrections could be important, while axial couplings due to the nuclear spin have less impact. In this picture, the CEvNS cross-section is given by [17]

$$\frac{\mathrm{d}\sigma}{\mathrm{d}T} = \frac{G_F^2 M}{\pi} g_c\left(1 - \frac{TM}{2E_\nu}\right) \cdot \sum_{f,f'} F_f F_{f'}^* \left[g_V^f g_V^{f'}\left(A_f A_{f'}\left(1 - \frac{y\tau}{2}\right)^2 + \Delta A_f \Delta A_{f'}\left(\frac{y}{2}\right)^2\right) + g_A^f g_A^{f'}\left(A_f A_{f'}\left(\frac{y\tau}{2}\right)^2 + \Delta A_f \Delta A_{f'}\left(1 - \frac{y}{2}\right)^2\right)\right.$$

$$+ 2g_V^f g_A^{f'} \left(A_f A_{f'} \left(1 - \frac{y\tau}{2}\right) \frac{y\tau}{2} + \Delta A_f \Delta A_{f'} \frac{y}{2} \left(1 - \frac{y}{2}\right)\right)\Bigg] \tag{6}$$

where the sums on both f and f' run over p and n, with $A_p = Z$, $A_n = N$, and ΔA_f is the difference between the corresponding nucleons with a spin projection along the incident neutrino axis and those with spin projection opposite to it, the Bjorken y is given by $y = T/E_\nu$ and s is the total energy squared. Finally, $\tau = (\sqrt{s} - m_N)/(\sqrt{s} + m_N)$, with m_N the nucleon mass. It has also been discussed in the same reference that the contributions due to ΔA_f and $g_A^f g_A^{f'}$ are small. We have checked that indeed, for the CsI cross-section, these corrections are at least three orders of magnitude smaller and, therefore, we will not consider them. After these approximations, (4) and (6) are still different by a factor g_c. This factor arises if we require [17] that the interaction of the incident neutrino happens only when the nucleon has an initial momentum $\vec{p} = -(\vec{q}/2)(1 - m_N/M)$ and acquires a final momentum $\vec{p} + \vec{q}$, with m_N the mass of the nucleon. In this picture, the factor g_c is given by the product of three different factors, two of which are of order unity, while the last one is reported to be linear in T [17]. Under this assumption, we found the factor g_c to be given by

$$g_c = 1 + \frac{MT}{m_N E_\nu}. \tag{7}$$

On the other hand, once we take an expression for the cross-section, the number of events measured by a detector is given by

$$N^{th} = N_D \int_T A(T)\, dT \int_{E_{min}}^{52.8MeV} dE\lambda\left(E_\nu, T\right) \frac{d\sigma}{dT}, \tag{8}$$

where $A(T)$ is an acceptance function, $\lambda(E_\nu, T)$ is the neutrino flux, and N_D is, depending on the detector, the number of targets in it and is given by $N_A M_{det}/M_D$, with N_A the Avogadro's number, M_{det} the mass of the detector, and M_D its molar mass. The limits of the T integral depend on both the detector's threshold and the maximum recoil energy for a fixed E_ν, which to our purposes is well approximated by $T_{\max}(E_\nu) \simeq 2E_\nu^2/M$. On the other hand, the integral over E_ν has an upper limit of 52.8 MeV, which corresponds to the maximum energy of the neutrinos coming from the SNS.

Before computing a forecast of the sensitivity to future new experiments, we have computed what would be the expected number of events in the case of the recent COHERENT detection of CEvNS for the previous two formulations of the cross-section. To this purpose, by closely following the procedure described in [3], we have computed the expected number of events by recoil energy bins for the case of the CsI detector using an average neutron rms radius of 5.5 fm for both Cs and I, which was found to be the best fit to the COHERENT data [3]; we take the acceptance function as given in [23]. Table 1 (see Introduction) shows the specific values for the detector's mass and its distance to the neutrino source.

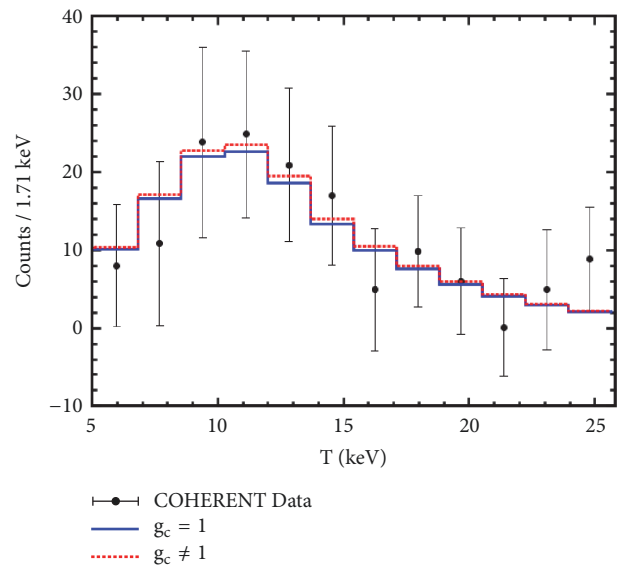

FIGURE 1: Expected number of events for the CsI COHERENT case. The solid (blue) line corresponds to the usual approach to the cross-section as given in (4) while the dotted (red) line corresponds to the more detailed case discussed in [17]. The points correspond to the experimental data [2].

The results of this computation are illustrated in Figure 1, where we show the expected number of events when we consider the cross-section as in (4) as well as when we consider the case of a linear kinematic correction due to the factor g_c. It is possible to notice that the introduction of the kinetic factor g_c yields to a relatively larger number of events. Despite the fact that this factor can introduce important corrections in the cross-section for high neutrino energies, the convolution of the neutrino energy spectrum and form factors translates into an increase of 5% or less in the total number of events for the targets under consideration. We have checked that this effect translates into a small shift in the central value of a given fit but has no impact in the width of the errors. Therefore, for our computations of the future expectations we will show the results obtained with the more simple and usual approach of (4).

Regarding future experiments, throughout the following sections we will study the cases of Ge, Ar and NaI detectors, which are reported by the COHERENT collaboration to start measuring CEvNS in the near future. Table 1 gives information about the estimated mass, threshold, and baseline on each case, all of which will be considered in our following computations to predict the current estimated number of events by using (8).

3. Sensitivity to the Weak Mixing Angle

Future CEvNS measurements will determine with accuracy the weak mixing angle value. Any deviation from

Table 2: Expected sensitivity, in percent, to the weak mixing angle. For each experiment we show the 90 % expected sensitivity for the different cases that we have considered.

Experiment	50 % eff σ_α = 5% σ_β = 10%	100% eff σ_α = 0% eff σ_β = 0% eff	100% eff σ_α = 15% σ_β = 10%	100% eff σ_α = 30% σ_β = 10%
Ge	11.5	7.2	17.5	36.8
Ar	5.5	1.5	15.6	35.6
NaI	5.2	1.2	15.0	34.2

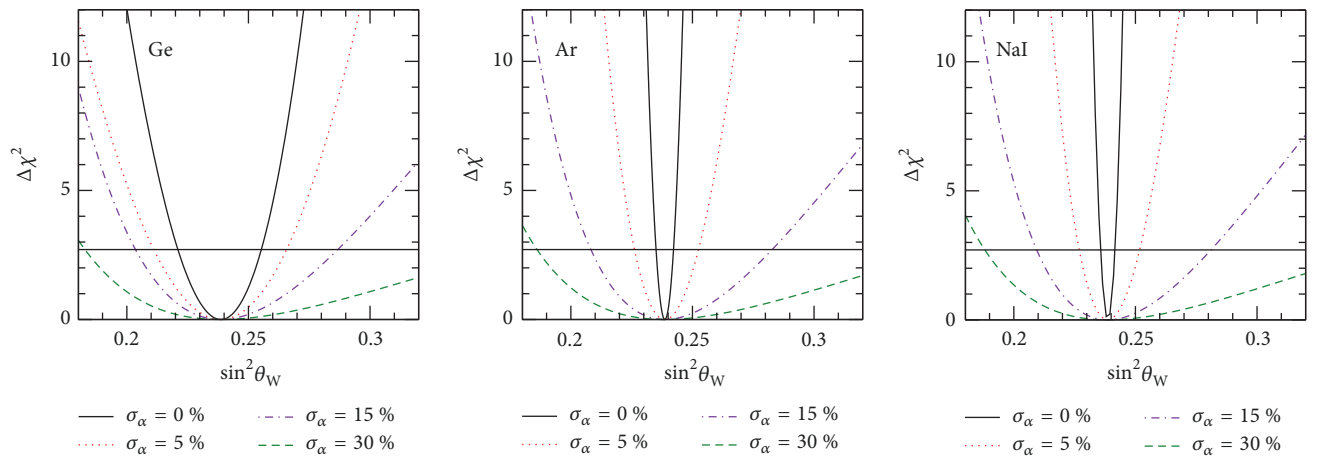

Figure 2: Expected sensitivity to $\sin^2\theta_W$ for the different detectors under consideration: Germanium, Argon, and NaI, respectively. The different curves are for the ideal case of σ_α = 0% with 100% efficiency and a background error of σ_β = 0% (solid), for σ_α = 5% with 50% efficiency and a background error of σ_β = 10% (dotted), for σ_α = 15% with 100% efficiency and a background error of σ_β = 10% (dashed-dotted), and σ_α = 30% with 100% efficiency and a background error of σ_β = 10% (dashed); see Table 2 and text for details. The horizontal line indicates the 90% CL.

the Standard Model prediction [24, 25] for this important quantity will be an indicator of new physics. Although the current estimates for the weak mixing angle from the CsI measurement are not competitive [6], future information from CEvNS may be of important relevance for this test of the SM at very low energies [4, 5]. For example, this information can be useful for the atomic parity violation (APV) measurement, where a small deviation from the prediction has been found [4]. As already mentioned, we have studied the future sensitivity to the weak mixing angle for the next generation of COHERENT experiments [10]. To this purpose, we have assumed that a futuristic χ^2 analysis will be given by the minimization of the function:

$$\chi^2 = \left(\frac{N^{exp} - (1+\alpha)\,N^{th}(X) - (1+\beta)\,N^{bg}}{\sigma}\right)^2 + \left(\frac{\alpha}{\sigma_\alpha}\right)^2 + \left(\frac{\beta}{\sigma_\beta}\right)^2, \quad (9)$$

where N^{exp} is the measured number of events, which, as we are dealing with a future experiment, we will consider as given by the SM prediction plus the expected background, $N^{th}(X)$ represents the predicted number of events as a function of a set of variable parameters X, which in this case corresponds only to the weak mixing angle, and N^{bg} is the expected background number of events, that we will consider to be ten percent of the predicted number of events; this background could come, for instance, from neutrino induced neutrons [26] or prompt neutrons [2]. This general expression will also be used in the following sections. The statistical uncertainty is given by $\sigma = \sqrt{N^{exp}}$, and the parameters α and β quantify the systematic errors with an associated uncertainty $\sigma_{\alpha,\beta}$.

The results are shown in Table 2 and Figure 2, where we have taken four different scenarios for each detector. These scenarios were considered in order to illustrate what would be the CEvNS sensitivity to this parameter. Regarding the systematic error σ_α, we can estimate that a first measurement could have large errors due to the normalization and quenching factor among other systematics [2]. Therefore we have considered a first scenario with σ_α = 30%, which is similar to the one reported by the first measurement reported by the COHERENT collaboration. A second case is that of σ_α = 15% that might be a realistic one after the detectors are better characterized. For the case of the background error we have considered it as 10%. We also show as a reference the very ideal case of no errors. Finally a different scenario with 50% efficiency and σ_α = 5%, σ_β = 10% is also considered. The expected sensitivity for the weak mixing angle (for symmetrized errors) is shown in Table 2, where we reported it at a 90% CL. With these different scenarios,

we expect to present a broad idea of the possible constraints that future experiments can obtain and what type of error would be more important to control. In all our computations we have considered an acceptance function equal to the unity for all T.

We can see from Table 2 and Figure 2 that, as expected, a detector with larger mass, such as the NaI case, will give better constraints, provided that the systematic errors are under control. In any case, even the more modest case of the Germanium detector with a 10 kg array could give a competitive measurement (for low energies) if the systematics can be maintained under control.

4. Sensitivity to NSI

Besides the precision tests of the Standard Model, there has been a lot of interest in different extensions of the SM to explain, for instance, the neutrino mass pattern. A useful phenomenological approach is that of nonstandard interactions (NSI) [27–29]. In general, neutral current nonstandard interactions can be parametrized by introducing a Lagrangian of the form

$$\mathfrak{L}_{\nu H}^{NSI} = -\frac{G_F}{\sqrt{2}} \sum_{\substack{q=u,d,\\ \alpha,\beta=e,\mu,\tau}} \left[\overline{\nu}_\alpha \gamma^\mu \left(1-\gamma^5\right)\nu_\beta\right] \cdot \left(\varepsilon_{\alpha\beta}^{qL}\left[\overline{q}\gamma_\mu\left(1-\gamma^5\right)q\right] + \varepsilon_{\alpha\beta}^{qR}\left[\overline{q}\gamma_\mu\left(1+\gamma^5\right)q\right]\right). \tag{10}$$

Here the interaction is modeled between the neutrino and the *up* and *down* quarks within the nucleons, so the index q runs over u and d. The subscripts α and β run over the three flavors e, μ, and τ. The Lagrangian in (10) contains flavor preserving, nonuniversal, nonstandard terms which are proportional to $\varepsilon_{\alpha\alpha}^{qV}$ (with $V = L, R$). Also, it contains the so-called flavor-changing terms proportional to $\varepsilon_{\alpha\beta}^{qV}$ with $\alpha \neq \beta$; all these coupling constants are taken in terms of the Fermi constant. Thus, for an electron (anti)neutrino source, the cross-section for $T << E_\nu$ now reads [19, 30–34]

$$\begin{aligned}\frac{d\sigma}{dT}(E_\nu, T) \simeq \frac{G_F^2 M}{\pi}\left(1-\frac{MT}{2E_\nu^2}\right)\Bigg\{&\left[Z\left(g_V^p + 2\varepsilon_{ee}^{uV} + \varepsilon_{ee}^{dV}\right)F_Z^V\left(Q^2\right) + N\left(g_V^n + \varepsilon_{ee}^{uV} + 2\varepsilon_{ee}^{dV}\right)F_N^V\left(Q^2\right)\right]^2 \\ &+ \sum_\alpha\left[Z\left(2\varepsilon_{\alpha e}^{uV} + \varepsilon_{\alpha e}^{dV}\right)F_Z^V\left(Q^2\right) + N\left(\varepsilon_{\alpha e}^{uV} + 2\varepsilon_{\alpha e}^{dV}\right)F_Z^V\left(Q^2\right)\right]^2\Bigg\}.\end{aligned} \tag{11}$$

The cross-section for a muon (anti)neutrino source has the same form and can be obtained by exchanging the indices $e \longleftrightarrow \mu$. For simplicity, here we will only consider the possibility of having NSI interactions coming from the electron neutrino source; this is a natural choice since the muon NSI parameters are usually more restricted from other experiments [27–29]. This means that the number of events measured by a detector at the SNS will be given by

$$N^{th} = N_D \int_T A(T)\, dT \int_{E_{min}}^{52.8MeV} dE \sum_a \frac{dN_a}{dE}\frac{d\sigma_a}{dT}, \tag{12}$$

where $a = \overline{\nu}_\mu, \nu_\mu, \nu_e$, with $d\sigma_a/dT$ given by (11) for $a = \nu_e$ and by (4) for the other two cases.

The study of the sensitivity to the NSI parameters is of relevance since any positive signal will hint for new physics; on the other hand, constraints on these parameters will potentially discard models of new physics. This is the case, for instance, for the first measurement of CEvNS where the reported constraints [2, 6, 8, 9] disfavored a class of models [35, 36] that were motivated by the Dark-LMA solution [37–40]. Future constraints from COHERENT collaboration will allow setting stronger constraints on the NSI parameters. The use of intense neutrino sources close to a CEvNS detector allows for a powerful setup that strongly constraints NSI parameters, competitive with any other neutrino experiment as already pointed out in Refs. [19, 30]

As in the previous section, we have studied the potential of the future setups for the SNS and computed the expected sensitivity for the different future detectors that are to be installed. We first made the analysis considering only one NSI parameter to be nonzero at a time. Although the parameters are correlated, this will give a first idea of the constraints that can be obtained and could be useful when we expect only small deviations from zero from a given new physics model [41, 42]. We will end up this section with a two-parameter analysis. Again, we have computed the χ^2 analysis of (9) with N^{th} given by (12) and X representing the corresponding NSI parameter. This time we have also considered the four different scenarios for the futuristic systematic uncertainties as in the previous section. Figure 3 shows the results for $\varepsilon_{\tau e}^{uV}$, while Figure 4 shows the corresponding results for ε_{ee}^{uV}. We can notice that, for the case of nonuniversal parameters, there are two different intervals where the ε_{ee}^{uV} values can lie. This is a well-known degeneracy that appears in the CEvNS case [30]. We show the numerical restrictions for both the flavor-changing and nonuniversal parameters in Tables 3 and 4, respectively. As in the previous section, we can see the importance of systematic errors, efficiency, and the mass of the detector. For example, we can notice that, for the case of a two tons NaI detector, the sensitivity is such that, even with a 30% error, the experiment can tell between the two degenerate allowed regions for ε_{ee}^{uV}, as can be seen in Table 4.

We close this section by illustrating one of the degeneracies that can appear if we consider more than one NSI parameter different from zero [19, 30]. For the case of considering both ε_{ee}^{uV} and $\varepsilon_{e\tau}^{uV}$ different from zero, we can notice from (11) that there is degeneration in the determination of this parameters that give rise to an ellipse, in analogy with [19]. We illustrate this case in Figure 5, where we can see that for this specific combination of parameters the detectors are unable to remove the degeneracy.

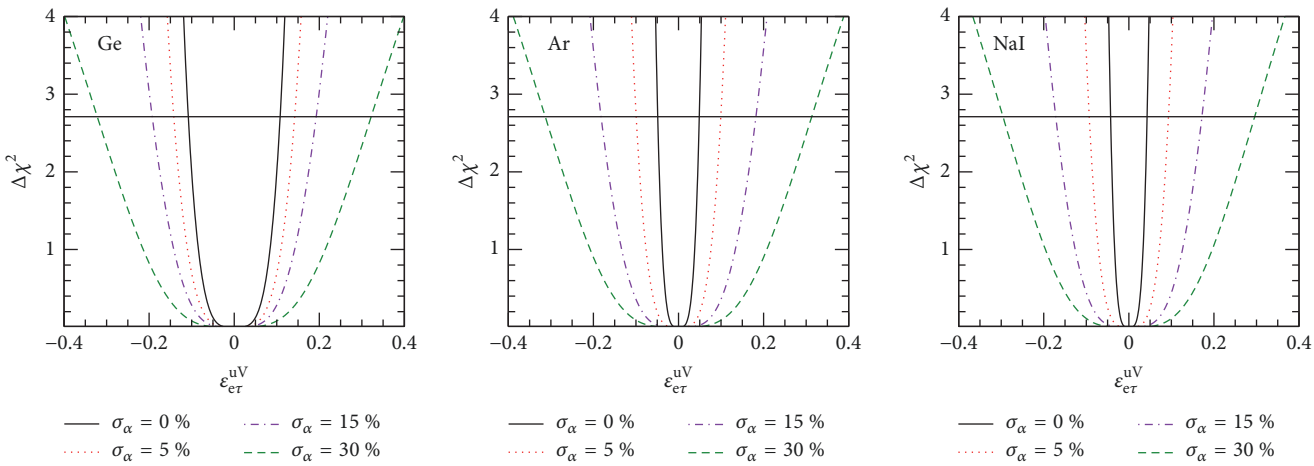

FIGURE 3: Expected sensitivity to $\varepsilon_{e\tau}^{uV}$ for the different detectors under consideration: Germanium, Argon, and NaI, respectively. Again, the different curves are for the ideal case of $\sigma_\alpha = 0\%$ with 100% efficiency and a background error of $\sigma_\beta = 0\%$ (solid), for $\sigma_\alpha = 5\%$ with 50% efficiency and a background error of $\sigma_\beta = 10\%$ (dotted), for $\sigma_\alpha = 15\%$ with 100% efficiency and a background error of $\sigma_\beta = 10\%$ (dashed-dotted), and $\sigma_\alpha = 30\%$ with 100% efficiency and a background error of $\sigma_\beta = 10\%$ (dashed); see text for details. The horizontal line indicates the 90% CL.

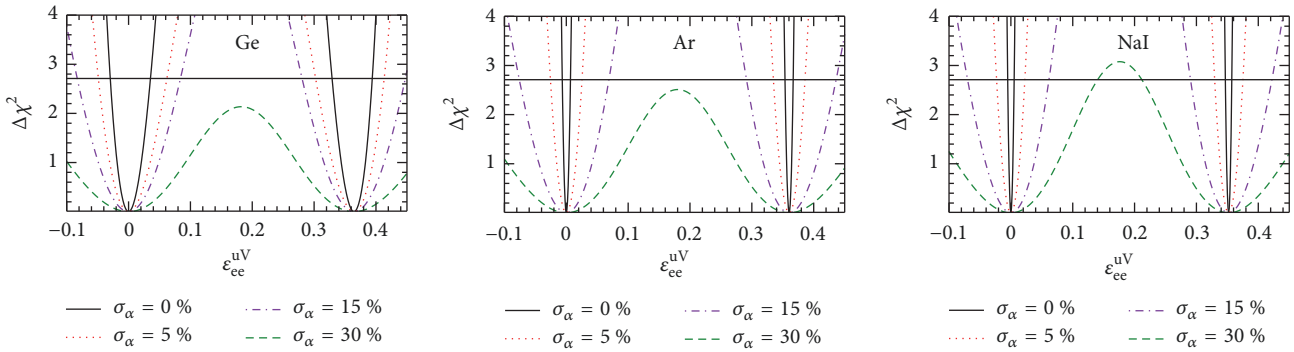

FIGURE 4: Expected sensitivity to ε_{ee}^{uV} for the different detectors under consideration: Germanium, Argon, and NaI, respectively. As in previous cases, the different curves are for the ideal case of $\sigma_\alpha = 0\%$ with 100% efficiency and a background error of $\sigma_\beta = 0\%$ (solid), for $\sigma_\alpha = 5\%$ with 50% efficiency and a background error of $\sigma_\beta = 10\%$ (dotted), for $\sigma_\alpha = 15\%$ with 100% efficiency and a background error of $\sigma_\beta = 10\%$ (dashed-dotted), and $\sigma_\alpha = 30\%$ with 100% efficiency and a background error of $\sigma_\beta = 10\%$ (dashed); see text for details. The horizontal line indicates the 90% CL.

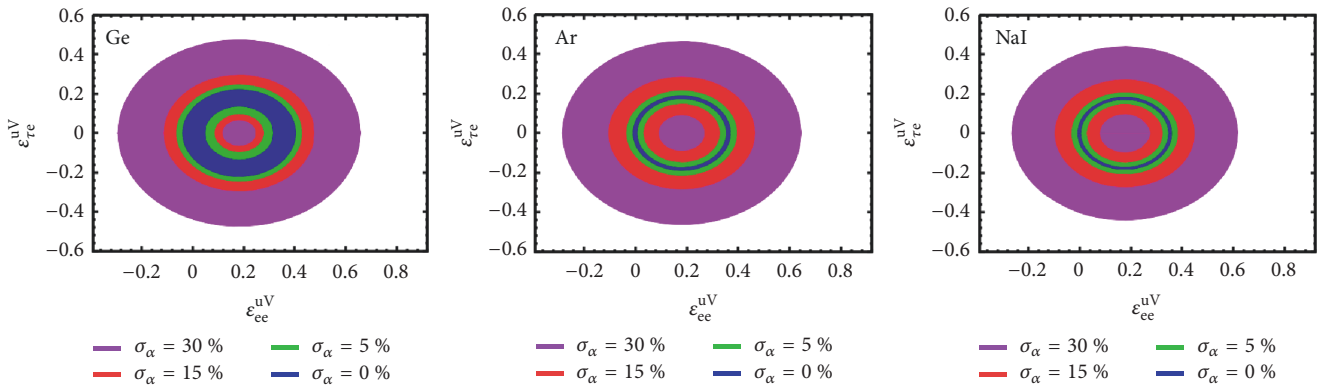

FIGURE 5: Expected sensitivity to ε_{ee}^{uV} vs. $\varepsilon_{e\tau}^{uV}$, at 90% CL for the different detectors under consideration: Germanium, Argon, and NaI, respectively. As in previous cases, the different curves are for the ideal case of $\sigma_\alpha = 0\%$ with 100% efficiency and a background error of $\sigma_\beta = 0\%$ (blue), for $\sigma_\alpha = 5\%$ with 50% efficiency and a background error of $\sigma_\beta = 10\%$ (green), for $\sigma_\alpha = 15\%$ with 100% efficiency and a background error of $\sigma_\beta = 10\%$ (red), and $\sigma_\alpha = 30\%$ with 100% efficiency and a background error of $\sigma_\beta = 10\%$ (magenta); see text for details.

Table 3: Expected sensitivity to the flavor changing NSI parameter $\varepsilon_{\tau e}^{uV}$. For each experiment we quote the 90 % CL expected sensitivity for the different scenarios that we have considered.

Experiment	50 % eff	100% eff	100% eff	100% eff
	σ_α = 5%	σ_α = 0% eff	σ_α = 15%	σ_α = 30%
	σ_β = 10%	σ_β = 0% eff	σ_β = 10%	σ_β = 10%
Ge	$\lvert\varepsilon_{\tau e}^{uV}\rvert < 0.142$	$\lvert\varepsilon_{\tau e}^{uV}\rvert < 0.108$	$\lvert\varepsilon_{\tau e}^{uV}\rvert < 0.193$	$\lvert\varepsilon_{\tau e}^{uV}\rvert < 0.322$
Ar	$\lvert\varepsilon_{\tau e}^{uV}\rvert < 0.100$	$\lvert\varepsilon_{\tau e}^{uV}\rvert < 0.048$	$\lvert\varepsilon_{\tau e}^{uV}\rvert < 0.182$	$\lvert\varepsilon_{\tau e}^{uV}\rvert < 0.314$
NaI	$\lvert\varepsilon_{\tau e}^{uV}\rvert < 0.093$	$\lvert\varepsilon_{\tau e}^{uV}\rvert < 0.041$	$\lvert\varepsilon_{\tau e}^{uV}\rvert < 0.172$	$\lvert\varepsilon_{\tau e}^{uV}\rvert < 0.296$

Table 4: Expected sensitivity to the nonuniversal NSI parameter ε_{ee}^{uV}. For each experiment we quote the 90 % CL expected sensitivity for the different scenarios that we have considered.

Experiment	50 % eff	100% eff	100% eff	100% eff
	σ_α = 5%	σ_α = 0% eff	σ_α = 15%	σ_α = 30%
	σ_β = 10%	σ_β = 0% eff	σ_β = 10%	σ_β = 10%
Ge	$-0.049 < \varepsilon_{ee}^{uV} < 0.062$	$-0.030 < \varepsilon_{ee}^{uV} < 0.035$	$-0.083 < \varepsilon_{ee}^{uV} < 0.084$	$-0.188 < \varepsilon_{ee}^{uV} < 0.553$
	$0.302 < \varepsilon_{ee}^{uV} < 0.414$	$0.328 < \varepsilon_{ee}^{uV} < 0.394$	$0.28 < \varepsilon_{ee}^{uV} < 0.445$	
Ar	$-0.026 < \varepsilon_{ee}^{uV} < 0.026$	$-0.006 < \varepsilon_{ee}^{uV} < 0.007$	$-0.076 < \varepsilon_{ee}^{uV} < 0.069$	$-0.182 < \varepsilon_{ee}^{uV} < 0.542$
	$0.335 < \varepsilon_{ee}^{uV} < 0.386$	$0.353 < \varepsilon_{ee}^{uV} < 0.366$	$0.291 < \varepsilon_{ee}^{uV} < 0.437$	
NaI	$-0.023 < \varepsilon_{ee}^{uV} < 0.023$	$-0.004 < \varepsilon_{ee}^{uV} < 0.004$	$-0.070 < \varepsilon_{ee}^{uV} < 0.062$	$-0.169 < \varepsilon_{ee}^{uV} < 0.141$
	$0.329 < \varepsilon_{ee}^{uV} < 0.375$	$0.347 < \varepsilon_{ee}^{uV} < 0.356$	$0.290 < \varepsilon_{ee}^{uV} < 0.422$	$0.211 < \varepsilon_{ee}^{uV} < 0.521$

5. Sensitivity to the Sterile Neutrino Hypothesis

Currently, the three neutrino oscillation picture is well established and most of its parameters are well measured [43–45]. However, there are different neutrino flux anomalies that cannot be explained by considering neutrino oscillations between three neutrino flavors [46]. For instance, the LSND observes an appearance of a $\overline{\nu_e}$ on a $\overline{\nu_\mu}$ flux; MIniBoone measures an excess of ν_e and $\overline{\nu_e}$ that agrees with the LSND results. On the other hand, for electron antineutrinos, a disappearance of $\overline{\nu_e}$ is observed in experiments with reactor neutrinos. These effects may be explained by considering a fourth noninteracting, sterile neutrino flavor. Expected constraints, considering different experimental setups, have been considered for the CEvNS case [47–49].

By considering each neutrino flavor state as a linear combination of mass eigenstates

$$\nu_l = \sum_m U_{lm}\nu_m \tag{13}$$

where U is a unitary mixing matrix, we can find the oscillation probability to be given by [50]

$$P_{\nu_\alpha\nu_\beta} = \delta_{\alpha\beta} - 4\sum_{i>j} Re\left(U_{\alpha i}^* U_{\beta i} U_{\alpha j} U_{\beta j}^*\right)\sin^2\left(\Delta m_{ij}^2 \frac{L}{4E}\right) + 2\sum_{i>j} Im\left(U_{\alpha i}^* U_{\beta i} U_{\alpha j} U_{\beta j}^*\right)\sin\left(\Delta m_{ij}^2 \frac{L}{2E}\right) \tag{14}$$

where the Latin subscripts correspond to the mass eigenstates, and the Greek ones correspond to the e, μ, τ, s neutrino flavors, $\Delta m_{ij}^2 = m_i^2 - m_j^2$, L is the distance from the neutrino source to the detector, and E_ν is the neutrino energy. Assuming CPT invariance, the antineutrino case is found by interchanging each matrix element with its complex conjugate, resulting in a reverse of the signs.

Due to the short source to detector distance (~ 10 m) and to the SNS neutrino energy spectrum (~ 10 MeV), the oscillations between the three active states can be neglected. Therefore, the probability of oscillation from active to sterile states can be studied in a two-flavor approximation:

$$P_{\nu_\alpha\nu_s} = \sin^2 2\theta_{\alpha\beta}\sin^2\left(\frac{1.27\Delta m_{i4}^2 L}{E_\nu}\right). \tag{15}$$

For simplicity, we will consider two different cases: first, the oscillation from $\nu_e \longrightarrow \nu_s$ and then the corresponding case for muon (anti)neutrinos. To take into account the oscillation of the neutrinos produced at the SNS, we take the probability that the considered neutrino keeps the same flavor as

$$P_\alpha = 1 - \sin^2 2\theta_{\alpha\alpha}\sin^2\left(\frac{1.27\Delta m_{i4}^2 L}{E_\nu}\right) \tag{16}$$

and this oscillation probability is multiplied by the neutrino flux and integrated over the neutrino energy spectrum, so the total number of events expected is given in this two cases by

$$N^{th} = N_D \int_T A(T)\, dT \int_{E_{min}}^{52.8MeV} dE \cdot \sum_\alpha \frac{dN_\alpha}{dE} P_\alpha\left(\theta_{\alpha\alpha}, \Delta m_{i4}^2\right)\frac{d\sigma}{dT}, \tag{17}$$

where the fluxes for the different neutrino flavors, α, are defined by (1)-(3). As in the case of NSI, we considered a χ^2

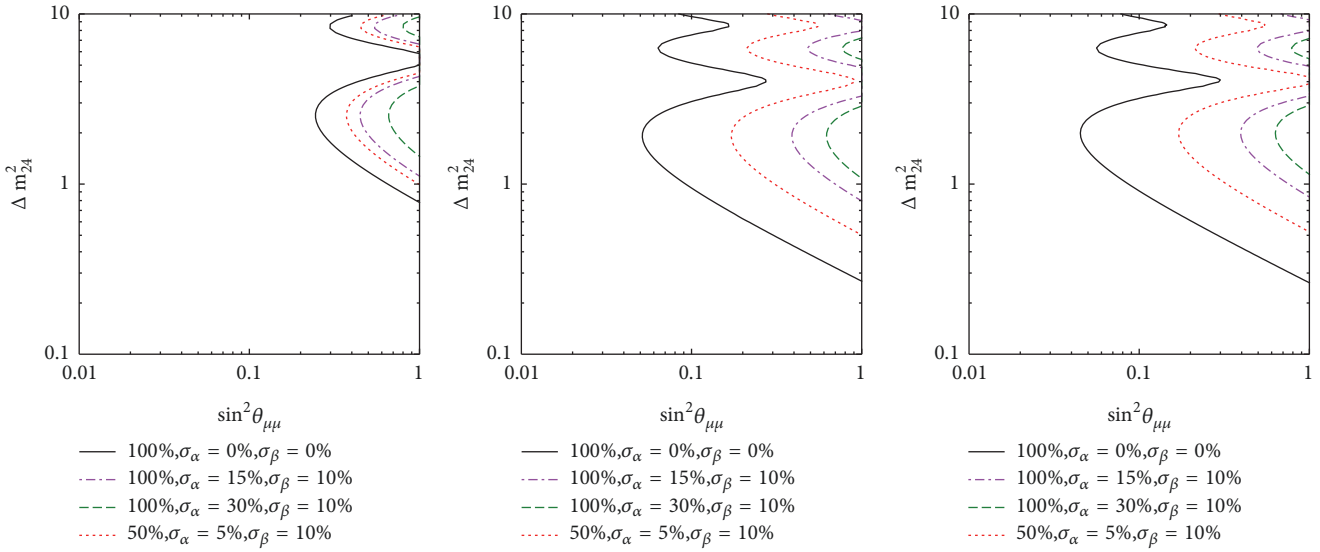

FIGURE 6: Expected sensitivity for a muon neutrino oscillation into a sterile neutrino state, for the different detectors under consideration: Germanium (left), Argon (middle), and NaI (right), respectively. Again, the different curves are for the ideal case of $\sigma_\alpha = 0\%$ with 100% efficiency and a background error of $\sigma_\beta = 0\%$ (solid), for $\sigma_\alpha = 5\%$ with 50% efficiency and a background error of $\sigma_\beta = 10\%$ (dotted), for $\sigma_\alpha = 15\%$ with 100% efficiency and a background error of $\sigma_\beta = 10\%$ (dashed-dotted), and $\sigma_\alpha = 30\%$ with 100% efficiency and a background error of $\sigma_\beta = 10\%$ (dashed); see text for details. The horizontal line indicates the 90% CL.

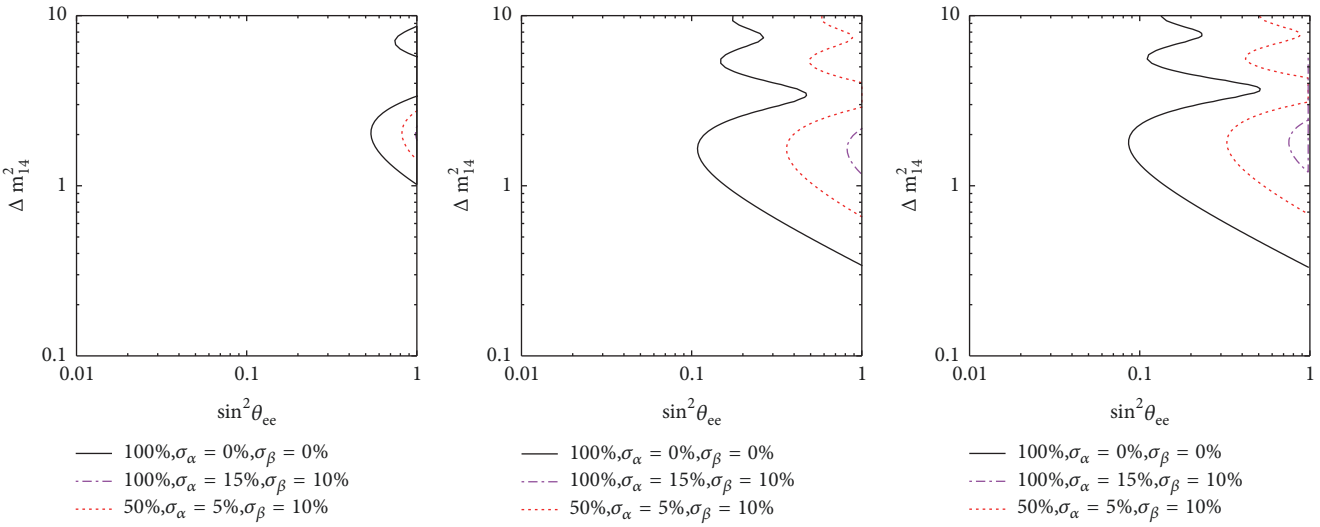

FIGURE 7: Expected sensitivity for an electron neutrino oscillation into a sterile neutrino state, for the different detectors under consideration: Germanium (left), Argon (middle), and NaI (right), respectively. Again, the different curves are for the ideal case of $\sigma_\alpha = 0\%$ with 100% efficiency and a background error of $\sigma_\beta = 0\%$ (solid), for $\sigma_\alpha = 5\%$ with 50% efficiency and a background error of $\sigma_\beta = 10\%$ (dotted), for $\sigma_\alpha = 15\%$ with 100% efficiency and a background error of $\sigma_\beta = 10\%$ (dashed-dotted), and $\sigma_\alpha = 30\%$ with 100% efficiency and a background error of $\sigma_\beta = 10\%$ (dashed); see text for details. The horizontal line indicates the 90% CL.

function in order to forecast the sensitivity of COHERENT future experiments. In this case, since neutrino oscillation probability is a function of two variables ($\sin^2 2\theta_{\alpha\alpha}, \Delta m^2_{i4}$), we will take the χ^2 function as the one described in (9) with $N^{th}(X) = N^{th}(\sin^2 2\theta_{\alpha\alpha}, \Delta m^2_{i4})$ as in (17).

For this case, our analysis considers only one parameter at a time. That is, we only consider either $\sin\theta_{ee}$ or $\sin\theta_{\mu\mu}$ different from zero and compute the corresponding effect in the electron (muon) neutrino number of events. In Figures 6 and 7 we show the sensitivity to the allowed regions of the parameters $\sin^2 2\theta_{\alpha\alpha}$ and Δm^2_{i4} for the different systematic errors and efficiencies that we have already discussed. The results are shown at 90% CL.

Although for some cases the expected sensitivity is not competitive, we can notice that for the more ambitious detectors with larger mass there is sensitivity to the relevant region of sterile neutrino searches.

6. Discussion and Conclusions

The measurement of CEvNS by the COHERENT collaboration has been a break through that opens the door to new measurements of this elusive process. Motivated by the future program of the same collaboration, we have studied the expected sensitivity for precision tests of the Standard Models as well as for new physics searches. We have focused on the case of the measurement of the weak mixing angle, the sensitivity to NSI, and the future constraints on a sterile neutrino state.

We have studied the different proposed detectors on equal footing, in the sense that we have considered the same total neutrino flux coming from the Spallation Neutron Source and we have also considered the same efficiencies and systematic errors. We have illustrated quantitatively that the most ambitious large mass detector arrays will give better constraints on new physics, provided that systematics are under control. We have also estimated the weakness of the constraints if the efficiency is compromised.

Data Availability

The data used to support the findings of this study are available from the corresponding author upon request.

Conflicts of Interest

The authors declare that they have no conflicts of interest.

Acknowledgments

This work was supported by CONACYT-Mexico under grant A1-S-23238 and by SNI (Sistema Nacional de Investigadores). O. G. Miranda would also like to thank COFI.

References

[1] D. Z. Freedman, "Coherent effects of a weak neutral current," *Physical Review D: Particles, Fields, Gravitation and Cosmology*, vol. 9, no. 5, pp. 1389–1392, 1974.

[2] D. Akimov, J. B. Albert, P. An et al., "Observation of Coherent Elastic Neutrino-Nucleus Scattering," *Science*, vol. 357, no. 6356, pp. 1123–1126, 2017.

[3] M. Cadeddu, C. Giunti, Y. F. Li, and Y. Y. Zhang, "Average csi neutron density distribution from coherent data," *Physical Review Letters*, vol. 120, Article ID 072501, 2018.

[4] M. Cadeddu and F. Dordei, "Reinterpreting the weak mixing angle from atomic parity violation in view of the Cs neutron rms radius measurement from COHERENT," *Physical Review D*, vol. 99, no. 3, p. 033010, 2019.

[5] X.-R. Huang and L.-W. Chen, "Neutron Skin in CsI and Low-Energy Effective Weak Mixing Angle from COHERENT Data," https://arxiv.org/abs/1902.07625.

[6] D. K. Papoulias and T. S. Kosmas, "COHERENT constraints to conventional and exotic neutrino physics," *Physical Review D*, vol. 97, no. 3, p. 033003, 2018.

[7] M. Cadeddu, C. Giunti, K. A. Kouzakov, Y. F. Li, A. I. Studenikin, and Y. Y. Zhang, "Neutrino Charge Radii from COHERENT Elastic Neutrino-Nucleus Scattering," *Physical Review D*, vol. 98, no. 11, p. 113010, 2018.

[8] P. Coloma, M. C. Gonzalez-Garcia, M. Maltoni, and T. Schwetz, "COHERENT enlightenment of the neutrino dark side," *Physical Review D*, vol. 96, Article ID 115007, 2017.

[9] J. Liao and D. Marfatia, "COHERENT constraints on nonstandard neutrino interactions," *Physics Letters B*, vol. 775, no. 54, 2017.

[10] D. Akimov, J. B. Albert, and P. An, "COHERENT 2018 at the Spallation Neutron Source," https://arxiv.org/abs/1803.09183.

[11] P. B. Denton, Y. Farzan, and I. M. Shoemaker, "Testing large non-standard neutrino interactions with arbitrary mediator mass after COHERENT data," *Journal of High Energy Physics*, vol. 7, no. 37, 2018.

[12] J. Billard, J. Johnston, and B. J. Kavanagh, "Prospects for exploring New Physics in Coherent Elastic Neutrino-Nucleus Scattering," *Journal of Cosmology and Astroparticle Physics*, vol. 2018, no. 11, p. 16, 2018.

[13] V. Brdar, W. Rodejohann, and X.-J. Xu, "Producing a new fermion in coherent elastic neutrino-nucleus scattering: from neutrino mass to dark matter," *Journal of High Energy Physics*, vol. 12, no. 24, 2018.

[14] W. Altmannshofer, M. Tammaro, and J. Zupan, "Non-standard neutrino interactions and low energy experiments," 1812.02778, 2018.

[15] D. Aristizabal Sierra, J. Liao, and D. Marfatia, "Impact of form factor uncertainties on interpretations of coherent elastic neutrino-nucleus scattering data," *Journal of High Energy Physics*, 2019.

[16] C. Blanco, D. Hooper, and P. Machado, "Constraining Sterile Neutrino Interpretations of the LSND and MiniBooNE Anomalies with Coherent Neutrino Scattering Experiments," 1901.08094, 2019.

[17] V. A. Bednyakov and D. V. Naumov, "Coherency and incoherency in neutrino-nucleus elastic and inelastic scattering," *Physical Review D*, vol. 98, no. 5, p. 053004, 2018.

[18] A. Drukier and L. Stodolsky, "Principles and applications of a neutral-current detector for neutrino physics and astronomy," *Physical Review D*, vol. 30, 1984.

[19] J. Barranco, O. G. Miranda, and T. I. Rashba, "Probing new physics with coherent neutrino scattering off nuclei," *Journal of High Energy Physics*, vol. 12, no. 21, 2005.

[20] K. Patton, J. Engel, G. C. McLaughlin, and N. Schunck, "Neutrino-nucleus coherent scattering as a probe of neutron density distributions," *Physical Review C*, vol. 86, Article ID 024612, 2012.

[21] D. K. Papoulias and T. S. Kosmas, "Standard and Nonstandard Neutrino-Nucleus Reactions Cross Sections and Event Rates to Neutrino Detection Experiments," *Advances in High Energy Physics*, vol. 2015, Article ID 763648, 17 pages, 2015.

[22] S. Zhou, "Update on two-zero textures of the majorana neutrino mass matrix in light of recent T2K, super-kamiokande and NO νA results," *Chinese Physics C*, vol. 40, no. 3, Article ID 033102, 2016.

[23] D. Akimov et al., "Producing a new fermion in coherent elastic neutrino-nucleus scattering: from neutrino mass to dark matter," *Journal of High Energy Physics*, 2018.

[24] M. Tanabashi et al., "Review of Particle Physics," *Physical Review D:*, vol. 98, Article ID 030001, 2018.

[25] J. Erler and R. Ferro-Hernandez, "Weak mixing angle in the thomson limit," *JHEP*, vol. 196, p. 20, 2017.

[26] T. Abbott, L. Ahle, and Y. Akiba, "Systematics of midrapidity transverse energy distributions in limited apertures from p+Beto Au+Au," *Physical Review C: Nuclear Physics*, vol. 63, Article ID 064602, 2001.

[27] Y. Farzan and M. Tórtola, "Neutrino oscillations and Non-Standard Interactions," *Frontiers in Physics*, vol. 6, 10 pages, 2018.

[28] F. F. Deppisch, P. S. Bhupal Dev, and A. Pilaftsis, "Neutrinos and collider physics," *New Journal of Physics* , vol. 17, no. 3, Article ID 036005, 2015.

[29] T. Ohlsson, "Status of non-standard neutrino interactions," *Reports on Progress in Physics*, vol. 76, no. 4, Article ID 044201, 2013.

[30] K. Scholberg, "Prospects for measuring coherent neutrino-nucleus elastic scattering at a stopped-pion neutrino source," *Physical Review D: Particles, Fields, Gravitation and Cosmology*, vol. 73, Article ID 033005, 2006.

[31] D. Aristizabal Sierra, V. De Romeri, and N. Rojas, "COHERENT analysis of neutrino generalized interactions," *Physical Review D*, vol. 98, Article ID 075018, 2018.

[32] J. B. Dent, B. Dutta, S. Liao, J. L. Newstead, L. E. Strigari, and J. W. Walker, "Accelerator and reactor complementarity in coherent neutrino-nucleus scattering," *Physical Review D*, vol. 97, Article ID 035009, 2018.

[33] M. Lindner, W. Rodejohann, and X.-J. Xu, "Coherent neutrino-nucleus scattering and new neutrino interactions," *Journal of High Energy Physics*, vol. 97, 2017.

[34] P. Coloma, P. B. Denton, M. C. Gonzalez-Garcia, M. Maltoni, and T. Schwetz, "Curtailing the dark side in non-standard neutrino interactions," *Journal of High Energy Physics*, vol. 116, 2017.

[35] Y. Farzan, "A model for large non-standard interactions of neutrinos leading to the LMA-Dark solution," *Physics Letters B*, vol. 748, pp. 311–315, 2015.

[36] Y. Farzan and I. M. Shoemaker, "Lepton flavor violating non-standard interactions via light mediators," *Journal of High Energy Physics*, vol. 33, 2016.

[37] O. G. Miranda, M. A. Tortola, and J. W. F. Valle, "Are solar neutrino oscillations robust?" *Journal of High Energy Physics*, vol. 10, no. 8, 2006.

[38] F. J. Escrihuela, O. G. Miranda, M. A. Tórtola, and J. W. Valle, " Erratum: Constraining nonstandard neutrino-quark interactions with solar, reactor, and accelerator data [Phys. Rev. D **80** , 105009 (2009)] ," *Physical Review D: Particles, Fields, Gravitation and Cosmology*, vol. 80, no. 12, 2009.

[39] P. Coloma and T. Schwetz, "Generalized mass ordering degeneracy in neutrino oscillation experiments," *Physical Review D*, vol. 94, Article ID 055005, 2017, [Erratum: Phys. Rev.D95,no.7,079903(2017)].

[40] M. C. Gonzalez-Garcia and M. Maltoni, "Determination of matter potential from global analysis of neutrino oscillation data," *Journal of High Energy Physics*, vol. 9, no. 152, 2013.

[41] J. W. F. Valle and J. C. Romao, *Neutrinos in high energy and astroparticle physics*, Physics textbook, Wiley-VCH, Weinheim, 2015, ISBN 9783527411979, 9783527671021, http://eu.wiley.com/WileyCDA/WileyTitle/productCd-3527411976.html.

[42] M. Fukugita and T. Yanagida, "Physics of neutrinos and application to astrophysics," *Theoretical and Mathematical Physics*, 2003.

[43] P. F. de Salas, D. V. Forero, C. A. Ternes, M. Tortola, and J. W. F. Valle, "Status of neutrino oscillations 2018: 3σ hint for normal mass ordering and improved CP sensitivity," *Physics Letters B*, vol. 782, pp. 633–640, 2018.

[44] F. Capozzi, E. Lisi, A. Marrone, and A. Palazzo, "Current unknowns in the three-neutrino framework," *Progress in Particle and Nuclear Physics*, vol. 102, pp. 48–72, 2018.

[45] M. C. Esteban, A. Gonzalez-Garcia, M. Hernandez-Cabezudo, Maltoni., and T. Schwetz, "Global analysis of three-flavour neutrino oscillations: synergies and tensions in the determination of θ_{23}, δ_{CP}, and the mass ordering," *Journal of High Energy Physics*, 2018.

[46] S. Gariazzo, C. Giunti, M. Laveder, Y. F. Li, and JHEP., "Updated global 3+1 analysis of short-baseline neutrino oscillations," *Journal of High Energy Physics*, vol. 135, 2017.

[47] B. Dutta, Y. Gao, R. Mahapatra et al., "Sensitivity to oscillation with a sterile fourth generation neutrino from ultralow threshold neutrino-nucleus coherent scattering," *Physical Review D*, vol. 94, Article ID 093002, 2016.

[48] T. S. Kosmas, D. K. Papoulias, M. Tortola, and J. W. F. Valle, "Probing light sterile neutrino signatures at reactor and Spallation Neutron Source neutrino experiments," *Physical Review D*, vol. 96, Article ID 063013, 2017.

[49] B. C. Canas, E. A. Garces, O. G. Miranda, and A. Parada, "The reactor antineutrino anomaly and low energy threshold neutrino experiments," *Physics Letters B*, vol. 776, pp. 451–456, 2018.

[50] C. Giunti and C. W. Kim, *Fundamentals of Neutrino Physics and Astrophysics*, 2007, ISBN 9780198508717.